Modified phonon confinement model for Raman spectroscopy of nanostructured materials

K. Roodenko,[1,*] I. A. Goldthorpe,[2] P. C. McIntyre,[2] and Y. J. Chabal[1]
[1]*Laboratory for Surface and Nanostructure Modification, Department of Material Science and Engineering, University of Texas Dallas, Richardson, Texas 75083, USA*
[2]*Materials Science and Engineering, Stanford University, Stanford, California 94305, USA*
(Received 19 December 2009; revised manuscript received 21 June 2010; published 20 September 2010)

This work describes further development of the confinement theory used for fitting of the Raman-spectroscopy signal obtained from nanostructured materials. We present a simple algebraic method for the incorporation of an anisotropic phonon-dispersion function into the phonon confinement model. The anisotropy is shown to have particular effects on low-dimensional systems, of sizes below ~15 nm, even for systems with low anisotropy such as Ge. Experimental verification of the model is provided by fitting the Raman signal from Ge nanowires grown on quartz substrates. The interplay between the temperature change due to Raman laser heating and the size of the nanostructures is discussed.

DOI: 10.1103/PhysRevB.82.115210 PACS number(s): 78.30.Er, 81.07.Gf, 81.05.Zx

I. INTRODUCTION

Raman spectroscopy is rapidly becoming a standard tool for the characterization of low-dimensional systems, such as quantum dots, nanowires, and microcrystalline structures.[1–3] Its popularity is due to the wealth of information that it can provide regarding nanostructures. For instance, one can deduce sample chemical composition, structure,[4] and physical properties such as thermal conductivity[5] of nanostructures based entirely on Raman spectra. Since the properties of bulk materials may differ from those of nanostructures, assignment of the Raman peak positions as well as peak shapes may require simulations and modeling.

The phonon mode calculations in nanostructures may require different modeling for polar and nonpolar materials. For example, Thonhauser and Mohan[6] have calculated the phonon spectrum in Si [111] nanowire and solved for eigenvectors in free-standing wires of several diameters. Fonoberov and Balandin[7] derived an integral equation within a dielectric-continuum model to show that, while the frequency of confined polar-optical phonons in zinc-blende nanocrystals is equal to that of the bulk crystal phonons, the confined polar-optical phonons in wurtzite nanocrystals have a discrete spectrum of frequencies different from those of the bulk crystal.

In addition, there are several theoretical models for simulations of Raman scattering that have been developed to interpret Raman spectra obtained on nanostructured materials. For example, Thonhauser and Mohan[8] use a bond-polarizability model with the eigenfrequencies obtained from spring-and-mass model of the Stillinger and Weber type[8] to calculate the ratio between the intensities of different polarizations. Based on such ratio, the nanowire diameter can be determined theoretically.

Another model, which has gained much popularity within the Raman community to describe nanostructured materials, is called the phonon confinement model. Although this model is somewhat simplistic, it can be reliably applied to fit the measured Raman data and to reproduce the position and width of the Raman peak obtained from nanostructured materials. This model was first formulated by Richter *et al.*[9] and expanded by Campbell and Fauchet.[10] A detailed account of this work was summarized by Fauchet and Campbell in 1988.[11] The authors recognized then that "this issue deserves further studies" due to several controversial results that arose from this model. The simplicity of the phonon confinement model [also commonly referred to as Richter-Cambell-Fauchet (RCF) model], and the need for a fast, nondestructive way to determine the size of nanostructures have stimulated the relatively frequent use of this model to study nanoscale materials.[2] However, inadequacies associated with this approach continue to be debated. For instance, some authors, such as Adu *et al.*,[12] have investigated possible reasons for the wide discrepancy found in the literature concerning the parameters used in the RCF model.

In this work, we undertake to resolve issues directly related to these discrepancies, such as the parameters used within the RCF model to describe the phonon-weighting function. We show that the problem stems from a misinterpretation of the phonon-weighting function that was initially proposed by Richter *et al.*[9] We note that the RCF model does not take into account surface effects and cannot predict Raman peaks arising from them, which can be done by models suggested, for example, in Refs. 6, 7, and 13. Instead, the strength of the RCF model is its ability to give a fast estimation of the nanostructure size, when it is applied properly, as well as to provide a means to determine the temperature that develops due to the Raman laser heating.[2,14]

In addition to resolving the problem of the phonon-weighting function, we show in this paper how the isotropic RCF model can be generalized for nanostructures fabricated from materials with *anisotropic* phonon-dispersion properties. This issue is of special importance for highly anisotropic materials such as titanium oxide, which possesses strongly anisotropic dispersion relations. This problem has previously been discussed in the literature.[15–18] One of the most elegant ways to solve the anisotropy problem was proposed by Paillard *et al.*[19] and involved averaging over phonon frequency using a Brout sum.[20] Our proposed approach does not involve averaging. Instead, following a purely algebraic approach, the calculation takes into account phonon dispersion in each relevant crystallographic direction. All the discussion presented here stays within the framework of the phonon

confinement model as proposed by Richter *et al.*,[9] which is based on the assumption that the bulk phonon dispersion holds in nanostructures.

II. RCF MODEL

A. Phonon weighting function

The RCF model is applied in cases where the Raman spectra are obtained not from an infinite lattice but rather from nanostructures with finite dimensions. Equation (1) describes a wave function for a phonon of wave vector $\mathbf{q}_0$ in an infinite crystal with a periodic function $u(\mathbf{q_0},\mathbf{r})$, where $\mathbf{r}$ is the space vector,

$$\Phi(\mathbf{q}_0,\mathbf{r}) = u(\mathbf{q}_0,\mathbf{r})e^{-i\mathbf{q}_0\mathbf{r}}. \tag{1}$$

Richter *et al.*[9] proposed to use a "phonon-weighting function" $W(\mathbf{r})$ to describe a phonon in a microcrystal with finite dimensions,

$$\Psi(\mathbf{q_0},\mathbf{r}) = W(\mathbf{r})\Phi(\mathbf{q_0},\mathbf{r}) = \Psi'(\mathbf{q_0},\mathbf{r})u(\mathbf{q_0},\mathbf{r}). \tag{2}$$

The typical choice of $W(r)$ is of a Gaussian $W(\mathbf{r})=\exp[-\mathbf{r}^2/(2^*\sigma^2)]$, where σ is a constant and matched individually for a given measurement setup and material[3,12] in accordance to the sample's dimensions. Initially, Richter *et al.*[9] proposed a Gaussian as an approximation to simplify the calculations of integrals [see Eqs. (3) and (8) which will be described in the following]. Current computational applications allow one to calculate exact integrals numerically, thus more precise phonon-weighting functions than Gaussian can be readily incorporated. In this work, we discuss incorporation of the precise phonon-weighting function, namely, the square wave, the reason for which will be discussed next. We compare this choice with the earlier proposed weighting functions and show that when the parameter σ of the Gaussian is chosen properly, both models give identical results. In addition, we show that current computational technology, where numerical integration can be carried out effectively, makes it possible to incorporate anisotropy into the RCF model, where Raman scattering from the relevant crystallographic planes can be taken into account. The model is tested against experimental results obtained from nanowire structures.

For a given $\Psi'(\mathbf{q}_0,r)$, the Fourier coefficient $C(\mathbf{q}_0,\mathbf{q})$ are then obtained in Eq. (3),

$$C(\mathbf{q}_0,\mathbf{q}) \sim \int d^3r\Psi'(q_0,\mathbf{r})e^{-i\mathbf{q}\cdot\mathbf{r}}. \tag{3}$$

For one-phonon scattering, $q_0=0$ is assumed.

For a Gaussian weighting function of the form $W(\mathbf{r})=\exp[-\mathbf{r}^2/(2^*\sigma^2)]$, the Fourier coefficient is in general of the form

$$|C(0,\mathbf{q})|^2 = \sim |\exp(-0.5\mathbf{q}^2\sigma^2)|^2. \tag{4}$$

The value of the parameter σ in the Gaussian is highly disputed in the literature (see, for example, values summarized by Adu *et al.*[12] from various literature sources). Adu *et al.*[12] have shown that any results can be calibrated to fit to the RCF theory, if the "universal parameter" σ is varied. In fact, the origin of this parameter lies in a proper choice of the spatial function $W(\mathbf{r})$ function (Fig. 1).

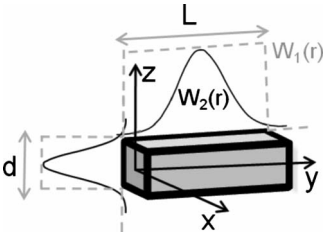

FIG. 1. Representation of a nanowire with the face size d and length L, and the respective weight functions $W_1(\mathbf{r})$ (square-wave function, dashed) and $W_2(\mathbf{r})$ (Gaussian, solid line).

In case of nanowires, it is intuitive to use square-wave function $W_1(\mathbf{r})$ (Fig. 1) to represent the nanowire in the Cartesian coordination system (x,y,z) in the following way:

$$W(x,d) = 1 \quad \text{for} \quad -d/2 < x < d/2,$$
$$\text{else} \quad W(x,d) = 0 \quad (\text{same for the } z \text{ direction}),$$
$$W(y,L) = 1 \quad \text{for} \quad -L/2 < y < L/2,$$
$$\text{else} \quad W(y,L) = 0. \tag{5}$$

This type of square-wave function confines the structure in space. The Fourier transform of the rectangular function is $\text{sinc}(\frac{qd/a}{2\pi})$, where $\text{sinc}(x)$ is defined through $\frac{\sin(\pi x)}{\pi x}$ and the parameter a is the crystal constant [the lattice size of Ge is $a=5.64$ Å (Ref. 21)]. In the majority of publications, the Gaussian form is chosen due to the simpler evaluation of integrals involved in the RCF model.[3,9,10] For the Gaussian to match the square-wave function, especially after the Fourier transform (which provides the "window" in q space for calculations), the standard deviation (σ) in the Gaussian $W(\mathbf{r})=\exp[-\mathbf{r}^2/(2^*\sigma^2)]$ should be equal to the distances of all points in the square wave from the center, normalized to the number of the points. In other words, the standard deviation for any confined shape with a characteristic size d in a given direction (x, y, or z) should be

$$\sigma = \sqrt{\langle x^2\rangle} = \sqrt{\frac{\int_{-d/2}^{d/2} x^2 dx}{\int_{-d/2}^{d/2} dx}} = \frac{d}{\sqrt{12}}. \tag{6}$$

Figure 2 shows a comparative plot for the Gaussian and the square-wave function in r space and in q space for σ from Eq. (6) with those from the literature.[9,10] The seminal papers by Richter *et al.*[9] and Campbell and Fauchet[10] gave different reasoning regarding the Gaussian width. In case of Richter *et al.*,[9] the authors suggested that the phonon amplitude falls to the value of $1/e$ at the crystallite boundary. In q space, the Gaussian built upon our procedure of "mapping" the Gaussian into a square-wave function in Eq. (6) falls completely on the major cycle of the Fourier-transformed square wave. The Gaussian proposed by Richter *et al.*[9] follows closely the Fourier-transformed square wave as well. On the other hand, Campbell and Fauchet[10] suggested that

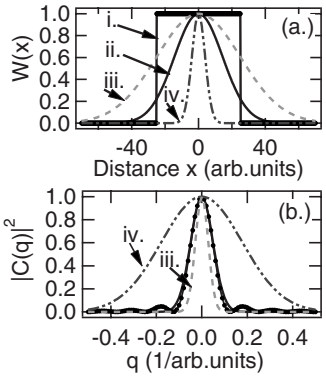

FIG. 2. (a) Phonon weighting function $W(x)$ calculated with $d=50$ arbitrary units. (i) square function; (ii) based on $W(x)=\exp[-x^2/(2^*\sigma^2)]$ with σ from Eq. (6); (iii) (dashed) Proposed by Richter *et al.* (Ref. 9); and (iv) (dashed-dotted) proposed by Campbell and Fauchet (Ref. 10). (b) The corresponding $|C(\mathbf{q})|^2$. Only the plots corresponding to plots (iv) and (iii) in (a) are marked, the rest of the lines fall closely together.

the phonon amplitude should be $\exp(-4\pi)$ at the boundary of the crystallite. This gives a much narrower window than the crystallite shape and results in a very wide Fourier-transformed Gaussian.

In order to compare this result to the results of the majority of other publications, we turn to the literature as summarized by Adu *et al.*[12] For their discussion, Adu *et al.*[12] use coefficient $|C(0,\mathbf{q})|$ of the following form:

$$|C(0,\mathbf{q})_{\mathrm{Adu}}|^2 = \sim \exp(-0.5\mathbf{q}^2d^2/\alpha^2). \tag{7}$$

To be consistent, we perform the comparison through the parameter α in Eq. (7). The relation between the parameters in Eqs. (4) and (7) is $\sigma^2=\frac{d^2}{2\alpha^2}$. A literature summary of the work of Adu *et al.*[12] gives reported results in the range $1.4<\alpha<10.4$, depending on the publication. The "universal value" for α found by Adu *et al.*[12] themselves is 6.3. To match between Eq. (7) and our Eq. (4) with $\sigma=d/\sqrt{12}$, the parameter α is $\alpha=\sqrt{6}=2.44$, in case of the properly confined Gaussian corresponding to the rectangular function. Table I shows a comparison between the Gaussian parameters used in various publications, this time in terms of the parameter σ where, for convenience, all literature Gaussian-based phonon confinement functions were converted into $|C(0,q)|^2=\sim|\exp(-0.5\mathbf{q}^2\sigma^2)|^2$ form.

TABLE I. Values of the Gaussian parameter σ in $|C(0,\mathbf{q})|^2=\sim|\exp(-0.5\mathbf{q}^2\sigma^2)|^2$ from this work and from different literature sources, where d is the parameter for nanostructure size in the phonon-weighting function.

σ	Literature source
$\frac{d}{2}$	Reference 9
$\frac{d}{4\pi}$	Reference 10
$\frac{d}{6.3\times\sqrt{2}}$	Reference 12
$\frac{d}{10.4\times\sqrt{2}}<\sigma<\frac{d}{1.4\times\sqrt{2}}$	Values summarized from the literature in Ref. 12
$\frac{d}{\sqrt{12}}$	This work, in accordance with Eq. (6)

It must be noted that despite these discrepancies, many authors who have applied the RCF model to the analysis of Raman data from nanowire samples have obtained reasonable results, which scaled with the size of the investigated nanostructures. Although the σ varied from publication to publication, the difference could be attributed to other parameters which influence the line shape of the measured Raman signal, such as strain and the induced heat within the nanostructure.[2]

In Sec. IV we fit our experimental data using square-wave weighting function [equivalent to the Gaussian phonon-weighting function with the parameter σ from Eq. (6)]. The fits will be presented after the discussion of the derivation of the dispersion equations for RCF model in anisotropic systems.

To summarize this part, we have shown that the controversy regarding the choice of parameters within the Gaussian confinement function in analysis of Raman line shapes measured from nanostructures can be resolved by consideration of the rectangular confinement function. The proper choice of the parameters within the Gaussian has been controversial since the publication of the RCF model in which Richter *et al.*[9] have used a weighting function of $W(r)=\exp(-2r^2/d^2)$ while Campbell and Fauchet have used $W(r)=\exp(-8\pi^2r^2/d^2)$, where d is the characteristic size of the nanostructure. In each case, the question was: to which value should the Gaussian function decay at the boundary of the crystallite? We have shown that the square wave sets clearly the proper boundary conditions at the edges of nanocrystallites. Our results set by a rectangular phonon confinement function are in closer agreement with the choice of Richter *et al.*,[9] who proposed that the Gaussian falls to the value of $1/e$ at the crystallite boundary.

In Sec. IV, we fit our Raman data using phonon-weighting function with the square profile. Ma *et al.*[22] indicate hexagonal cross section of the nanowires grown under experimental conditions similar to ours. We note that the weighting function with the square-wave profile is an approximation in this case.

B. Dispersion relations

The RCF model proposes the following Lorentzian form for fitting of a Raman signal:

$$I(w) \sim \int d^3q|C(0,\mathbf{q})|^2/\{[w-w_0(\mathbf{q})]^2+(\Gamma/2)^2\}, \tag{8}$$

where $w_0(\mathbf{q})$ is the phonon-dispersion function. It should be noted that many authors perform the integration over the $\mathbf{q}$ in the first Brillouin zone (BZ) (i.e., Refs. 2, 10, and 18). We point out that this is incorrect since the periodicity of the lattice is broken at the very moment when the weighting function (which is the "confinement function") $W(\mathbf{r})$ is introduced. Thus, the correct way is to integrate q from $-\infty$ to ∞. For small crystal shapes, where d is only several times bigger than the lattice parameter, the difference between integration over the BZ and from $-\infty$ to ∞ can become important. How-

TABLE II. Parameters used to fit the phonon dispersion using Eq. (9) for three major crystallographic axes in Ge. Two of the relevant axes in a nanowire are considered in ⟨110⟩ crystallographic directions.

Relevant mode	A_0 (cm^{-1})	A_1 (cm^{-1})	A_2 (cm^{-1})	A_3 (cm^{-1})	A_4 (cm^{-1})
⟨110⟩ TO	284.9	15.13	2.84	0.65	0.21
⟨001⟩ LO	286.3	24	−8.4	2.8	−0.9

ever, since the RCF model assumes the validity of bulk phonon dispersion for nanostructures, we discuss only sizes of nanostructures which are (roughly) at least ten times bigger than the lattice size of the bulk material. Under these conditions, the integration over the **q** in the first BZ is valid.

Also the form of $w_0(q)$ is somewhat controversial in the literature, where "an isotropic" dispersion function $w_0(q)$ is typically applied.[2,10] This may work when the crystal structure of the nanostructured material is known and is the same for all crystallographic planes of the investigated particles. Bassi *et al.*[18] discuss the importance of using $w_0(q_x,q_y,q_z)$ in an anisotropic crystal. For powders which can exhibit anisotropy of phonon dispersion, Paillard *et al.*[19] proposed a sum rule which averages over different phonon branches in all relevant crystal directions. We point out that this is a good approach only when all directions are considered to be equivalent. In the case of nanowires, however, there are different dimensions in various directions. Thus, weighting functions $W(\mathbf{r})$ with different parameters for nanostructure size are used for each space direction. Consequently, an average $w_0(\mathbf{q})$ is not the proper way to describe the system, although it was shown to work when the dispersion properties of materials are not highly anisotropic.[12,18] We note that another approach for averaging was proposed by Prosandeev *et al.*,[23] involving averaging over the possible crystallite directions using rotation invariants. This approach was useful to deal with the integral Raman intensities of powders. The approach discussed in this work is different: rather than averaging on the integral Raman intensities in various directions, it implicitly includes the phonon-dispersion function in several relevant crystallographic directions, under the assumption that the bulk phonon dispersion holds for nanostructures, and that the same surface-selection rules apply.

In summary, the importance of a proper $w_0(q_x,q_y,q_z)$ is twofold: first, it accounts for a strong anisotropy in anisotropic crystals, where the "isotropic" function $w_0(\mathbf{q})$ is simply inappropriate. Second, it accounts for dimensionality in crystals, where the appropriate length scales in the x, y, and z directions differ, as in nanowires.

In this section, we demonstrate a simple algebraic approach which allows one to include an anisotropic $w_0(q_x,q_y,q_z)$ in the RCF model. This approach is based on the following assumptions: (1) the derivation is performed in the framework of the RCF phonon confinement model, which assumes that the bulk phonon modes can be used to describe nanostructures. No surface modes are taken into account. (2) This derivation assumes that the Raman surface-selection rules, which are valid for bulk, hold for the nanostructures.

(3) This discussion includes only two major modes (LO and TO) as allowed by Raman surface-selection rules for appropriate surface orientations, respectively. These modes are interpolated for the construction of the $w_0(q_x,q_y,q_z)$ function.

With regards to the third assumption, the aim of this paper is to demonstrate the effects of the inclusion of the anisotropy into the RCF model. Two cases are considered: one where the Raman-scattering directions considered in ⟨001⟩ or ⟨110⟩ crystallographic directions. The other case considers Raman scattering in ⟨111⟩, ⟨112⟩, and ⟨110⟩ crystallographic directions. The derivation of the $w_0(q_x,q_y,q_z)$ for the latter case is given in the Appendix. We note that the formalism presented here allows one to include any modes that are likely to contribute to the Raman scattering in accordance to surface-selection rules.

In order to calculate $w_0(q_x,q_y,q_z)$, we match the boundary conditions for $w_0(\mathbf{q})$ in the three major crystallographic directions of the nanostructures under study. In our experiments, Ge NWs are oriented along the ⟨110⟩ axes. For simplicity, we choose to work in the Cartesian system of coordinates, approximating the shape of the NW as a rectangular box.

In the following, we choose dispersion relations in three orthogonal directions, namely, [110], [001], and $[1\bar{1}0]$. The bulk phonon dispersion in Ge along these three high-symmetry directions are readily available from literature.[24,25] Presently, based on the backscattering geometry in our experiments, we follow the Raman selection rules[4] that dictate that for backscattering from {001} planes the allowed phonon mode is LO polarized and for the backscattering from {110} is TO polarized.

First, we write an analytical form for the dispersion in bulk Ge using data from Ref. 24 by the following Fourier-type expansion. We fit on data from[24] using Eq. (9),

$$w(q) = A_0 + \sum_n A_n \cos(n\pi q). \tag{9}$$

The parameter q in Eq. (9) is the normalized parameter of the reciprocal lattice. The obtained parameter values for Eq. (9) are summarized in Table II and represented in Fig. 3.

The step presented below [Eqs. (10), (11a)–(11c), and (12)] is used to calculate $w_0(q)$ which is a three-dimensional (3D) form for $w_0(q_1,q_2,q_3)$ where q_1, q_2, and q_3 are the wave-vector parameters in the [110], [001], and $[1\bar{1}0]$ directions. (Our particular choice stems from the fact that the Ge NWs that are discussed in the experimental section were grown along the ⟨110⟩ direction.) This $w_0(q_1,q_2,q_3)$ is the function which appears in Eq. (8) and is required for simulations of the Raman signal. The general form of the $w_0(q_1,q_2,q_3)$ basically involves a superposition of three

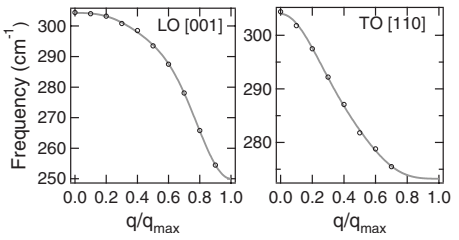

FIG. 3. Dispersion relations for the TO and LO modes allowed in a backscattering geometry by the Raman selection rules in ⟨001⟩ and ⟨110⟩ directions. Black circles: data from Ref. 24 (at 80 K), gray line: fit obtained by the curve of the type presented by Eq. (9).

properly parametrized forms of Eq. (9) to accommodate the three possible solutions for $w_{110}(q_1)$, $w_{001}(q_2)$, and $w_{1\bar{1}0}(q_3)$,

$$w_0(q_1,q_2,q_3) = C_0 + \sum_{i=1}^{3}\sum_{n=1}^{\infty} C_n^i \cos(n\pi q_i), \tag{10}$$

where we have performed an expansion up to $n=4$. The 13 coefficients of cos functions are obtained by solving 13 boundary equations as discussed next.

The function given in Eq. (10) is defined through fulfilling the following conditions:

$$w_0(q_1,0,0) = w_{110}(q_1), \tag{11a}$$

$$w_0(0,q_2,0) = w_{1\bar{1}0}(q_2), \tag{11b}$$

$$w_0(0,0,q_3) = w_{001}(q_3), \tag{11c}$$

where $w_{110}(q_1)$, $w_{1\bar{1}0}(q_2)$, and $w_{001}(q_3)$ are given by Eq. (9) with the appropriate parameters from Table II.

To obtain $w_0(q_1,q_2,q_3)$ it is required to solve boundary equations which would fulfill the common boundary conditions,

$$w_0(0,0,0) = \text{constant} = w_{110}(q_1=0) = w_{1\bar{1}0}(q_2=0) = w_{001}(q_3=0) \tag{12}$$

at the Γ point of the first Brillouin zone. This constitutes the first necessary boundary equation (out of 13), and Eqs. (11a)–(11c) constitute the remaining 12 necessary equations for any arbitrary point q between 0 and 1 in the normalized wave-vector space (or, more generally, in the first Brillouin zone), in order to obtain the parameters of Eq. (10).

In our case, where q_1, q_2, and q_3 are the wave-vector parameters are in the [110], [1$\bar{1}$0], and [001] directions, the parameters summarized in Table III were obtained. Parameters summarized in Table III constitute the solution for Eq. (10) and can be readily used for anisotropic materials (with major axes [110], [1$\bar{1}$0], and [001]) in Eq. (8). The resultant reconstructed anisotropic phonon-dispersion function is shown in Fig. 4.

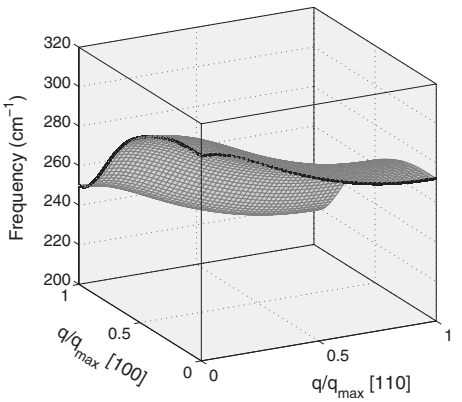

FIG. 4. Anisotropic phonon-dispersion function $w(q_{110},q_{1\bar{1}0},q_{001})$ represented as a function of q_{001}, q_{110} where $q_{1\bar{1}0}$ was set to zero. The phonon-dispersion functions $w_{100}(q)$ and $w_{110}(q)$ are marked in black.

C. Application

In this section, we test the use of isotropic vs anisotropic phonon-dispersion functions and discuss the influences of the preferential nanowire growth directions on the Raman spectra. Since our Raman setup and the samples (as will be presented in Sec. IV) allow us to perform measurements on single nanowires rather than on nanowire ensembles, we do not take into account any size distribution effects throughout this work. Thus, in this section (as well as in Sec. IV) we discuss simulations based on a discrete size of a single nanostructure.

It is interesting to address several nanocomposite structures, to demonstrate how the RCF model changes when anisotropy is applied on different structures. Figure 5 shows several test shapes on which the application of the modified RCF model will be discussed in the following.

1. Nanodots

In this section, we compare the results of the RCF calculations as obtained for a one-dimensional $w(q)$ and an aniso-

TABLE III. Parameters obtained for the construction of anisotropic phonon-dispersion function $w(q_{110},q_{1\bar{1}0},q_{001})$. The coefficients represent the parameters in Eq. (10) with the boundary conditions of Eqs. (11) and (12). The data are presented with the room-temperature adjustments.

Relevant i mode in C_i^n	C_0 (cm^{-1})	C_1^i (cm^{-1})	C_2^i (cm^{-1})	C_3^i (cm^{-1})	C_4^i (cm^{-1})
$i=1$	251	15	3.15	0.53	0.37
$i=2$		15	3.15	0.53	0.37
$i=3$		24	−8.4	2.9	−0.95

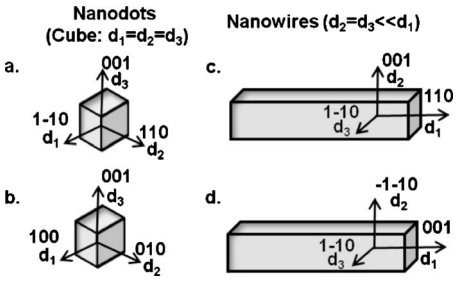

FIG. 5. Schematic drawing of hypothetical nanostructures with different geometries and orientations. In this work, the RCF model with the relevant anisotropy is applied to simulate Raman signal from each of the nanostructures.

tropic $w(q_1,q_2,q_3)$. The isotropic calculations were performed using the "radial" form of Eq. (8). This type of approximation is frequently performed in the literature.[2,12,18] For instance, in the case of quantum dots, the integration of d^3q is reduced to q^2dq while for the nanowires, where the inequality nanowire length $\gg$ short facet diameter holds, the integration over d^3q is reduced to qdq. In this case, a one-dimensional form of $w(q)$ is used. An anisotropic calculation with $w(q_1,q_2,q_3)$, on the other hand, was performed using Eq. (8) with d^3q integration over q_1, q_2, and q_3.

It is interesting to test how the *crystallographic orientation* influences the theoretical Raman signal both in d^3q and q^2dq models. Thus, for q^2dq case the calculations were performed with the phonon-dispersion function $w(q)$ in both the $\langle 001\rangle$ or $\langle 110\rangle$ crystallographic directions (Fig. 5) while for the d^3q model, the $w(q_1,q_2,q_3)$ was implemented as calculated from Eqs. (10), (11a)–(11c), and (12), both in the three {001} equivalent directions or along the [110], $[1\bar{1}0]$, and [001] orthogonal directions. For simplicity, we refer to the latter calculation as "[110] d^3q" calculation hereafter, although the [001] direction is involved in this case as well. We do not show a derivation of the $w(q_{001},q_{010},q_{100})$ phonon function since it is straightforward when Eqs. (10), (11a)–(11c), and (12) are implemented.

In addition, Eq. (8) was modified to account for the local laser heating so that it can be later used in the fitting of the measured data,

$$I(w) \sim \int d^3q |C(0,\mathbf{q})|^2 / \{[w - w_0(\mathbf{q},T)]^2 + [\Gamma(T)/2]^2\}, \tag{13}$$

where T is the temperature which develops due to the local heating and $w_0(q,T)$ is given by[26–28]

$$w(T) = w_0 + w_0\left(\exp\left\{-3\gamma\int_0^{T0}\alpha(T')dT'\right\} - 1\right) + A\left(1 + \frac{2}{e^x - 1}\right), \tag{14}$$

where $\alpha(T)$ is the coefficient of linear thermal expansion, γ is the mode Grueneisen parameter,[27] and $x=\hbar w_0(q)/(2K_BT)$, where K_B is the Boltzmann constant and T is the total temperature of the irradiated spot.[26] Similarly, $\Gamma(T)$ is given by[26,28]

$$\Gamma(T) = B\left[1 + \left(\frac{2}{e^x - 1}\right)\right] + B'\left[1 + \left(\frac{3}{e^y - 1}\right) + \frac{3}{(e^y - 1)^2}\right], \tag{15}$$

with x defined as before and $y=\hbar w_0(q)/(3K_BT)$.[26,28] In this case, the parameter B' is kept constant at a value published for c-Ge by Burke *et al.*[26] ($B'=0.06$ cm^{-1}) while the parameter B is retrieved from the fits as will be described in Sec. III. For nanostructures, the following average parameters as obtained from bulk c-Ge were used: $A=-1.2\pm0.2$ cm^{-1} and $B=0.75\pm0.15$ cm^{-1}, (see Sec. III B for details). For comparison, parameters A and B for bulk c-Ge as given by Burke *et al.*[26] where $A=-1.4$ cm^{-1} and $B=0.73$ cm^{-1}. In the following simulations, the parameter for temperature was kept identical so that it will be possible to compare between the outputs of the simulations. At this stage, the choice of this parameter can be somewhat arbitrary. We used $T_{laser}=50$ °C. However, for the fits of the measured Raman data, the influence of the temperature T_{laser} will be discussed separately in Sec. IV.

Figure 6 shows the results of the simulations. For bulk material, all simulations converge to the same result [Fig. 6(c)] since $w(\mathbf{q})$ contributes only at small q ($q\cong0$). For the nanodots with a diameter of 20 nm [Fig. 6(b)], the d^3q and q^2dq integrals give the same results in case of the phonon-dispersion function in {001} directions (labeled as "[001]" in Fig. 6). In case of $w(q_{110},q_{1\bar{1}0},q_{001})$ (labeled in Fig. 6 as [110] for simplicity), the results of the simulations fall close to the results obtained using the isotropic dispersion function $w(q_{110})$, although they do not coincide due to the influence of the phonon mode in [001] direction in the d^3q model.

Finally, for the smaller shapes [$d=5$ nm, Fig. 6(a)], the calculations for q^2dq and d^3q follow the line of the $d=20$ nm results. As before, a good agreement is obtained between the q^2dq and d^3q models for the dispersion relations in $\langle 001\rangle$ directions but the simulated results for the $w(q_{110},q_{1\bar{1}0},q_{001})$ give a higher asymmetry than the results of the simulations with the isotropic q^2dq model with the phonon dispersion in [110] direction due to the involvement of the [001] phonon mode in the anisotropic d^3q model.

To conclude this section, we point out that the 3D representation of the phonon function $w(q_1,q_2,q_3)$ is important for nanodots where the growth axis is such that different crystallographic planes contribute to the Raman signal. In the case of nanodots with {001} planes, when the dispersion function is equivalent in all directions, the q^2dq and d^3q models give identical results.

2. Nanowires

To compare between the d^3q model for anisotropy and the qdq model (as reduced from the d^3q integration for the nanowires and a frequently used in literature to fit Raman data[12,18]), we perform simulations for nanowires with the principal axes along [001], [110], and $[1\bar{1}0]$ directions, where the longitudinal axis is either along $\langle 001\rangle$ or $\langle 110\rangle$ (Fig. 7).

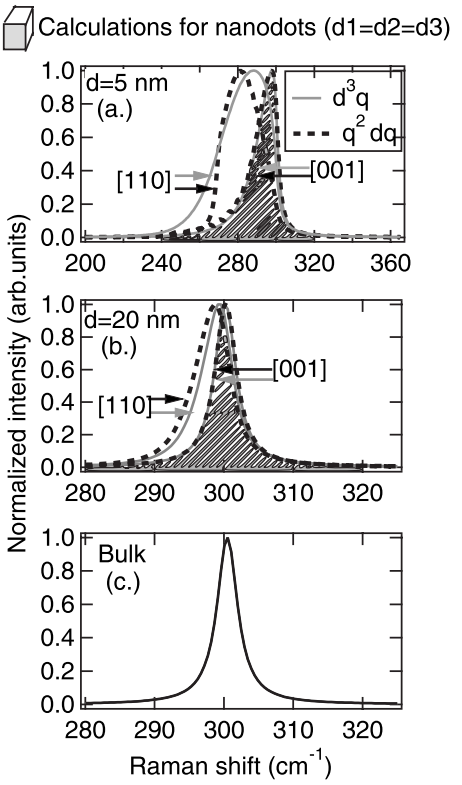

FIG. 6. Calculated Raman peaks using the RCF theory for different cube diameters: (a) 5 nm; (b) 20 nm; and (c) bulk. Black, dashed: one-dimensional (isotropic) calculation using q^2dq calculations for $w(q)$ in either $\langle 001\rangle$ or $\langle 110\rangle$ directions, as labeled in the figure. Gray, solid: 3D (d^3q) calculation with $w(q_1,q_2,q_3)$ all along the three $\langle 001\rangle$ equivalent directions (labeled as [001]) or along [110], [1$\bar{1}$0], and [001] crystallographic directions (labeled as [110]). In (c), all of the plots overlap. In (a) and (b), the peak area was shaded as a visual aid.

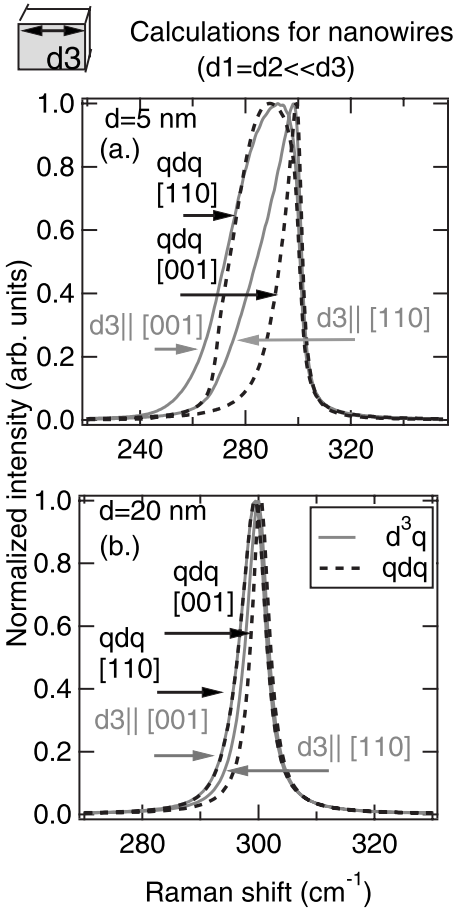

FIG. 7. Calculated Raman peaks with the RCF theory for different NW ($d1=d2\ll d3$) diameters: (a) $d_1=d_2=5$ nm and (b) $d_1=d_2=20$ nm. Black, dashed: one-dimensional (isotropic) calculation using qdq calculations for $w(q)$ in either $\langle 001\rangle$ or $\langle 110\rangle$ directions, as marked in the figure. Gray: 3D d^3q calculation with $w(q_1,q_2,q_3)$ with (001), (110), and (1$\bar{1}$0) crystallographic planes, where the longitudinal axis (d_3) is either parallel to the [001] or [110] direction.

For nanowires with a small diameter ($d=5$ nm), both the isotropic qdq model and the anisotropic d^3q model show a big difference in the shape of the signal depending on the dispersion function, $w(q)$. The calculations for the isotropic qdq model with $w(q)$ for the allowed phonon mode in the (110) crystallographic plane follows more closely the results of the d^3q calculations where the long dimension is along [001] direction [the two short dimensions being along the (1$\bar{1}$0) and (110) facets] but it is less asymmetric toward lower wave numbers. The similarity in this case is because the $\langle 110\rangle$ phonon mode is predominant both in d^3q and in qdq models while the phonon mode in [001] in d^3q model is positioned along the long dimension of the nanowire and contributes only close to $q=0$. For the nanowires with bigger diameters, the difference between the simulations utilizing different models (with similar crystallographic considerations) almost vanishes [Fig. 7(b)].

From the simulations it is evident that the asymmetry observed in previous studies[12] might also be due to anisotropy. The fact that this had not been noticed earlier may result from the difficulty of tuning the predicted broadening parameter Γ in Eq. (8) or may be a consequence of the nanowire growth axis. These considerations indicate that care should be taken and the crystallographic orientation of three-dimensional nanostructures should be accounted for in attempts to analyze the size of the nanostructures from Raman spectra using the RCF model.

Finally, we compare between crystallographically differently oriented nanowires within the d^3q model for anisotropy. For the shorter faces of the nanowire, we use the dispersion function $w(q_1,q_2,q_3)$ interpolated from the phonon-dispersion modes either along $\langle 001\rangle$ and $\langle 110\rangle$ or $\langle 111\rangle$ and $\langle 112\rangle$ crystallographic axes. We assume the growth axis along the $\langle 110\rangle$ directions in both cases. In Sec. IV, these two cases are used for fitting to the measured Raman data. Derivation of $w(q_1,q_2,q_3)$ in the latter case is presented in the Appendix.

Figure 8 shows the results of the simulations for nanowires of 9 nm diameter [Fig. 8(a)] and for bulk Ge [Fig. 8(b)]. The simulations were performed for the room temperature, assuming no additional heating during exposure to the laser. As expected, there are no differences in Raman signal simulated for bulk Ge. As the size becomes smaller, the de-

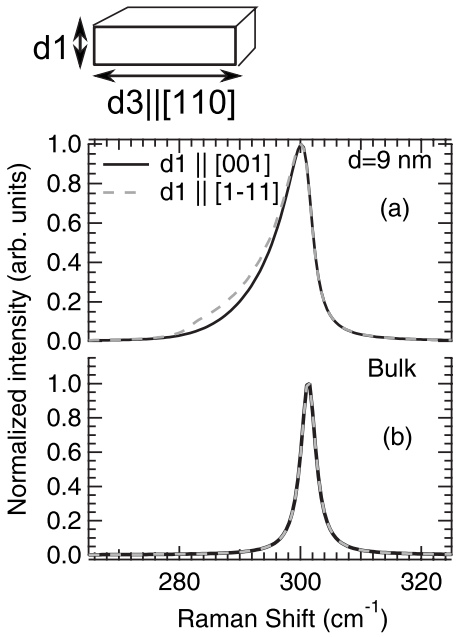

FIG. 8. Raman signal simulated for (a) 9 nm diameter nanowires and (b) for bulk. The long dimension of the nanowire is assumed along ⟨110⟩ crystallographic directions in both cases. Dashed line: the shorter faces were assumed along $(1\bar{1}1)$ and $(1\bar{1}\bar{2})$ planes; Solid line: the shorter faces were assumed along (001), $(1\bar{1}0)$ crystallographic planes (see the inset drawing).

viations in the simulated signals become observable. However, as will be shown in Sec. IV, when both dispersion functions are comparatively applied to fit the same Raman data, these effects are not significant within the nanowire diameter range of our experimental data.

III. EXPERIMENTAL

A. Sample preparation and Raman characterization

Germanium nanowires were grown on quartz substrates by chemical vapor deposition through the vapor-liquid-solid mechanism.[29] 5 nm gold nanoparticles were used as catalysts and germane was the source gas. The nanowires were nucleated at 370 °C for 2 min and the temperature was reduced to 310 °C for the remaining 25 min of growth. The pressure in the reactor was maintained at 30 Torr. Under these conditions, the nanowires grow predominantly along the ⟨110⟩ directions and have cross sections consisting of six surface facets: four {111}-type planes and two {100}-type planes.[22]

Because the substrate is amorphous, the nanowires have random spatial orientations. The wires grown using the 5 nm gold catalysts can be seen in Fig. 9. Based on measurements from scanning electron microscopy (SEM) images such as Fig. 9, the diameter of the Ge nanowires is 4 nm greater than the nominal catalyst diameter, with an uncertainty of ±3 nm.[30] Nanowires grown by the vapor-liquid-solid method are frequently found to have a larger diameter than that of the initial solid catalyst particles from which they grow because of the volume expansion accompanying supersaturation of the catalyst by the nanowire component (in this case Ge) and the resulting eutectic melting event.[30,31]

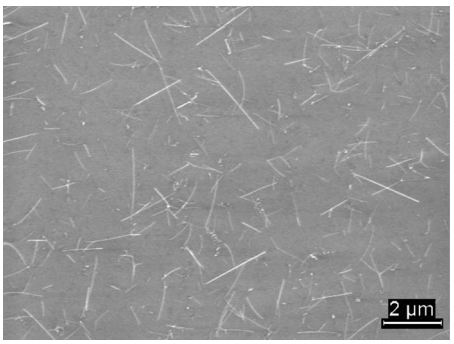

FIG. 9. Secondary electron microscopy image of germanium nanowires nucleated with 5 nm (nominal) diameter gold nanoparticles on a quartz substrate.

Samples with Ge nanowires on quartz were measured with a Nicolet Almega XR dispersive Raman spectrometer from Thermofisher. The spectra were obtained with a 532 nm laser at 0.045 mW power as measured at the sample plane. The Raman spectrometer was equipped with a microscope, where the 100× objective (NA 0.80) was utilized.

Due to the fact that the phonon-weighting function, describing hexagonal profile predicted for the nanowires, requires extensive numerical simulations, we used a square-wave profile as an approximation. We tested the effects of scattering both from {111} and from {100}-types planes, to be consistent with the findings by Ma *et al.*[22] In each case, the construction of the $w(q_1,q_2,q_3)$ phonon dispersion was dictated by the orientation of the long axis of the nanowire along ⟨110⟩ directions and the requirement of orthogonality. Two different phonon-dispersion functions—namely, $w(q_{110},q_{1\bar{1}0},q_{001})$ and $w(q_{110},q_{1\bar{1}1},q_{1\bar{1}\bar{2}})$—were used to describe the experimental data where the Raman radiation scatters from either {111}- or {001}-type planes. The derivation of $w(q_1,q_2,q_3)$ for the latter case is given in the Appendix. As demonstrated in the next section, the difference in the fitted parameters for the nanostructure size was insignificant when either of the dispersion functions was used.

For discussion of the quality of fits presented in the next section, we performed a mean squared error (MSE) test,[32] defined as

$$\mathrm{MSE} = \sqrt{\frac{1}{N-M}\sum_{j=1}^{N}(I_j^{\mathrm{fit}} - I_j^{\mathrm{experimental}})^2}, \qquad (16)$$

where N is the number of the points in the Raman data, M is the number of varied fit parameters, and I is the Raman intensity at each wave number.

B. Estimation of the parameters *A* and *B* in Eqs. (14) and (15)

Typically, the parameters A and B are extracted from the measurements of bulk properties of a material. For better statistics, we obtained Raman data on c-Ge in a set of measurements where the microfocus was scanned across different locations on c-Ge surface. The RCF model with the dimension $d \to \infty$ was fitted to each Raman peak (not shown).

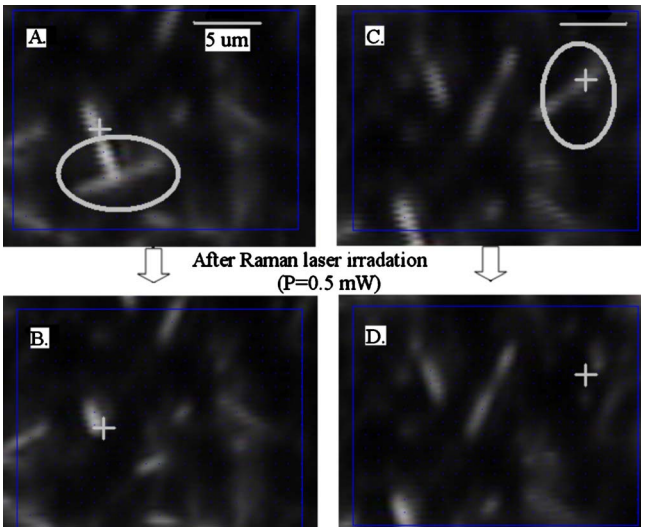

FIG. 10. (Color online) Laser damage of Ge nanowires on quartz surfaces. [(A) and (C)]: before Raman laser irradiation; [(B) and (D)] after the irradiation. For B, a 532 nm laser was used while for D, a 780 nm laser resulted in the same outcome. The region of interest is marked by a circle. After irradiation, the nanowire could no longer be seen. All pictures are shown to the same scale (the scale bar is 5 μm).

Thus for c-Ge, we obtained $A=-1.2\pm0.2$ cm^{-1} and $B=0.75\pm0.15$ cm^{-1}. The published data vary between $A=-1.4$ cm^{-1} (Ref. 26) and $A=-1.13$ cm^{-1},[27] whereas the detailed analysis as well as the literature summary regarding the variations in these parameters can be found in Ref. 27.

IV. RESULTS

The importance of local heating is demonstrated in Fig. 10. Upon irradiation with 0.5 mW laser power (either 532 or 780 nm wavelength), Ge nanowires of 45 nm in diameter sustained significant morphological damage. In all the following data the laser power was reduced to 0.045 mW, where no damage was detected with the optical microscope.

Based on this damage analysis and on the recognition that heating of nanostructures occurs during Raman measurements (see, for example, reports by Piscanec *et al.*[2] and Faraci *et al.*[14]), we included temperature as one of the parameters when fitting on the Raman data using the phonon-confinement RCF model.

Figure 11 shows two typical sets of measured data along with the resulting fits for the 9 ± 3 nm nanowires (as determined from SEM). Two Raman spectra obtained at two different spots in the sample are shown. The fits are presented for calculations utilizing $w(q_{110},q_{1\bar{1}0},q_{001})$ dispersion function. The best fits were obtained for 9.5 ± 2 nm [Fig. 11(a)] and for 11 ± 2 nm [Fig. 11(b)]. The best temperature fits were 370 K for the first spot and 375 K for the second. The accuracy in temperature estimation is discussed in the following.

We note that when the fits were performed with $w(q_{110},q_{1\bar{1}1},q_{1\bar{1}\bar{2}})$ dispersion function, only a slight deviation from the above data was observed [within 10% of the nanostructure size and temperature values calculated with $w(q_{110},q_{1\bar{1}0},q_{001})$]. The best fit converged with similar MSE values (less than 1% difference in MSE).

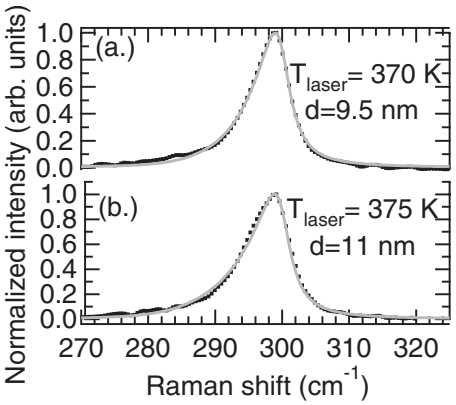

FIG. 11. Nanowires with SEM-estimated value of $d=9\pm3$ nm. Raman spectra on (a) and (b) were obtained at two different spots on the same sample. Dotted line: measured data; gray solid line: fitted data. The convergence of the relevant fit parameters is shown in Fig. 12. The spot temperature and the nanowire diameter are summarized in the figure area.

In order to test the interplay between the temperature and the nanowire size and to estimate the accuracy, Fig. 12 shows the convergence of the MSE and of the nanowire diameter as a function of the fixed temperature upon fitting on the data presented in Fig. 11. The data summarized in Fig. 12 show that there is a clear minimum in MSE in both cases. Shaded areas emphasize the regions where MSE varies within 10% around its minimum value. If we set the sensitivity threshold at 10% MSE variation, we obtain from Fig. 11(a) a nanowire diameter of 9.5 nm with accuracy of ±0.5 nm. Similarly, the temperature varies within ±20 K around its optimal value of 370 K.

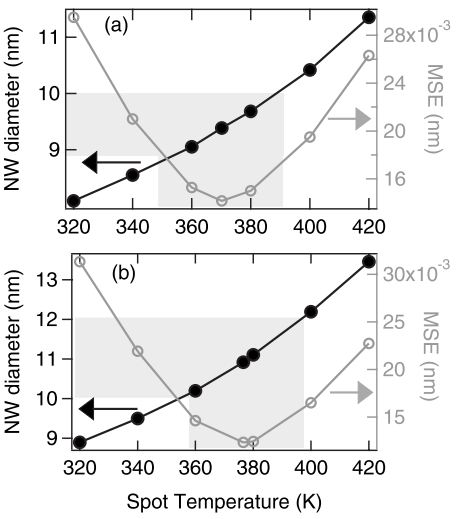

FIG. 12. Convergence of MSE and the development of nanowire diameter as a function of fixed temperature in the fit. (a) Variations in the fitted diameter and MSE for spectrum (a) in Fig. 11 and (b) variations in the respective parameters for spectrum (b) in Fig. 11. The shaded areas emphasize region of the possible solutions, where MSE changes within 10%.

For the set of data shown in Fig. 11(b), the criterion of 10% MSE variation similarly falls within the temperature range of ± 20 K, with a center at $T=375$ K. The diameter d can be determined as 11 ± 1 nm.

Application of the RCF model to additional Raman data sets, obtained from different nanowires on the sample, allowed us to estimate an average value for nanowire diameter and the variance. The average value was $d=10 \pm 2$ nm, which is in a good agreement with the SEM-estimated value of 9 ± 3 nm.

To summarize this section, we have performed fits using the improved phonon confinement model on nanowires with SEM value of $d=9 \pm 3$ nm. We tested the interplay between the temperature and the size estimation, based on the MSE analysis. The MSE shows a clear minimum for a certain range of the diameter/temperature parameters, and the derived nanostructure size is within the error bars of the SEM-measured values. Advanced temperature sensing techniques from confined spots, such as those based on near-field radiometry,[33] can be implemented in the future for cross referencing the data with the presented analysis.

V. CONCLUSIONS

In this work we have presented a way to improve the RCF model by (a) pointing out the proper choice of parameters in the Gaussian confinement function and by (b) introducing an anisotropic dispersion function into the confinement model. This demonstrates that anisotropy is of a particular importance for low-dimensional systems, where the broadening of the signal is strongly affected by the phonon dispersion of the material. The model has been tested on Ge nanowires with diameter less than 15 nm, where the fitted diameter values using our modified model were found to be in a good agreement with the values obtained from SEM analysis.

The tests performed on the interplay between the nanowire size and the temperature arising from local Raman heating show that the fit to the temperature/nanowire size is unique. On average, the fit converges best in the diameter range of $d=10 \pm 2$ nm for Ge nanowires with SEM-determined diameter of $d=9 \pm 3$ nm. Data analysis based on MSE evaluation show that the temperature arising from laser heating cannot be estimated to better than ± 20 K.

ACKNOWLEDGMENTS

K.R. would like to express gratitude to Ehud Fuchs for his valuable suggestions and guidance. This work was supported by NSF (Grant No. CHE-0911197), the Intel Foundation (I. A. G.), and by the Global Climate Energy Project at Stanford.

APPENDIX: CALCULATION OF ANISOTROPIC PHONON DISPERSION $w(q_{1\bar{1}1}, q_{1\bar{1}\bar{2}}, q_{110})$

The anisotropic phonon-dispersion function $w(q_{1\bar{1}1}, q_{1\bar{1}\bar{2}}, q_{110})$ was calculated following the derivation given in Sec. II B. Due to the surface-selection rules, we required that the backscattering in the $[1\bar{1}1]$ direction results in 2/3 of the TO intensity and 1/3 of the LO intensity.[4] The anisotropic phonon-dispersion function $w(q_{1\bar{1}1}, q_{1\bar{1}\bar{2}}, q_{110})$ is required to fulfill the following set of equations:

$$w_0(q,0,0) = w_{1\bar{1}1}(q), \tag{A1a}$$

$$w_0(0,q,0) = w_{1\bar{1}\bar{2}}(q), \tag{A1b}$$

$$w_0(0,0,q) = w_{110}(q). \tag{A1c}$$

Equation (A1b) is problematic since $\langle 112 \rangle$ directions are not along any principle high-symmetry axes. Thus, a reconstruction from properly set boundary conditions is required. To do this, we performed extrapolation by setting proper boundary conditions using the known dispersion relations along the high-symmetry crystallographic axes.

First, we rewrite Eq. (10) in the following form:

$$w_0(q_{1\bar{1}1}, q_{1\bar{1}\bar{2}}, q_{110}) = C_0 + \sum_{i=1}^{3} \sum_{n=1}^{\infty} C_n^i \cos[n\pi q_i'(q_{1\bar{1}1}, q_{1\bar{1}\bar{2}}, q_{110})], \tag{A2}$$

where, as before, we performed an expansion up to $n=4$. The variables q_i' are the linear combinations of $q_{1\bar{1}1}$, $q_{1\bar{1}\bar{2}}$, and q_{110},

$$q_1' = q_{1\bar{1}1} - 2q_{1\bar{1}\bar{2}}, \tag{A3a}$$

$$q_2' = q_{1\bar{1}1} + q_{1\bar{1}\bar{2}}, \tag{A3b}$$

$$q_3' = q_{110}. \tag{A3c}$$

This change in variables allows us to set the following boundary conditions with the proper periodicity along the principle crystallographic directions:

$$w_0(q,0,0) = w_{1\bar{1}1}(q), \tag{A4a}$$

$$w_0\left(\frac{q}{3}, -\frac{q}{3}, 0\right) = w_{001}(q), \tag{A4b}$$

$$w_0(0,0,q) = w_{110}(q). \tag{A4c}$$

Equations (A4a)–(A4c) allow to solve for coefficients C_i^n in Eq. (A2). Thus, $w(q_{1\bar{1}1}, q_{1\bar{1}\bar{2}}, q_{110})$ which fulfills Eqs. (A1a)–(A1c) is constructed. As before, throughout this paper we used LO phonon dispersion in $\langle 001 \rangle$ and TO in $\langle 110 \rangle$ crystallographic directions.

*Corresponding author; katy.roodenko@utdallas.edu

[1] G. Gouadec and P. Colomban, Prog. Cryst. Growth Charact. Mater. **53**, 1 (2007).
[2] S. Piscanec, M. Cantoro, A. C. Ferrari, J. A. Zapien, Y. Lifshitz, S. T. Lee, S. Hofmann, and J. Robertson, Phys. Rev. B **68**, 241312 (2003).
[3] A. K. Arora, M. Rajalakshmi, T. R. Ravindran, and V. Sivasubramanian, J. Raman Spectrosc. **38**, 604 (2007).
[4] P. Yu and M. Cardona, *Fundamentals of Semiconductors* (Springer-Verlag, Berlin, 1999).
[5] A. A. Balandin, S. Ghosh, W. Z. Bao, I. Calizo, D. Teweldebrhan, F. Miao, and C. N. Lau, Nano Lett. **8**, 902 (2008).
[6] T. Thonhauser and G. D. Mahan, Phys. Rev. B **69**, 075213 (2004).
[7] V. A. Fonoberov and A. A. Balandin, Phys. Rev. B **70**, 195410 (2004).
[8] T. Thonhauser and G. D. Mahan, Phys. Rev. B **71**, 081307(R) (2005).
[9] H. Richter, Z. P. Wang, and L. Ley, Solid State Commun. **39**, 625 (1981).
[10] I. H. Campbell and P. M. Fauchet, Solid State Commun. **58**, 739 (1986).
[11] P. M. Fauchet and I. H. Campbell, CRC Crit. Rev. Solid State Mater. Sci. **14**, s79 (1988).
[12] K. W. Adu, H. R. Gutierrez, U. J. Kim, G. U. Sumanasekera, and P. C. Eklund, Nano Lett. **5**, 409 (2005).
[13] C. Nobile, V. A. Fonoberov, S. Kudera, A. Della Torre, A. Ruffino, G. Chilla, T. Kipp, D. Heitmann, L. Manna, R. Cingolani, A. A. Balandin, and R. Krahne, Nano Lett. **7**, 476 (2007).
[14] G. Faraci, S. Gibilisco, and A. R. Pennisi, Phys. Rev. B **80**, 193410 (2009).
[15] M. J. Šćepanović, M. Grujić-Brojčin, Z. D. Dohčević-Mitrović, and V. Popović, Appl. Phys. A: Mater. Sci. Process. **86**, 365 (2007).
[16] A. Wellner, V. Paillard, C. Bonafos, H. Coffin, A. Claverie, B. Schmidt, and K. H. Heinig, J. Appl. Phys. **94**, 5639 (2003).
[17] V. Paillard, P. Puech, R. Sirvin, S. Hamma, and P. R. I. Cabarrocas, J. Appl. Phys. **90**, 3276 (2001).
[18] A. Li Bassi *et al.*, J. Appl. Phys. **98**, 074305 (2005).
[19] V. Paillard, P. Puech, M. A. Laguna, R. Carles, B. Kohn, and F. Huisken, J. Appl. Phys. **86**, 1921 (1999).
[20] R. Brout, Phys. Rev. **113**, 43 (1959).
[21] M. Jaros and K. W. Vinsome, J. Phys. C **2**, 2373 (1969).
[22] D. D. D. Ma, C. S. Lee, F. C. K. Au, S. Y. Tong, and S. T. Lee, Science **299**, 1874 (2003).
[23] S. A. Prosandeev, U. Waghmare, I. Levin, and J. Maslar, Phys. Rev. B **71**, 214307 (2005).
[24] G. Nilsson and G. Nelin, Phys. Rev. B **3**, 364 (1971).
[25] R. Tubino, G. Zerbi, and L. Piseri, J. Chem. Phys. **56**, 1022 (1972).
[26] H. H. Burke and I. P. Herman, Phys. Rev. B **48**, 15016 (1993).
[27] H. Tang and I. P. Herman, Phys. Rev. B **43**, 2299 (1991).
[28] M. Balkanski, R. F. Wallis, and E. Haro, Phys. Rev. B **28**, 1928 (1983).
[29] J. H. Woodruff, J. B. Ratchford, I. A. Goldthorpe, P. C. McIntyre, and C. E. D. Chidsey, Nano Lett. **7**, 1637 (2007).
[30] For a typical diameter distribution of chemical-vapor deposition-grown semiconductor nanowires see Y. Cui, J. Lauhon, M. S. Gudiksen, J. Wang, C. M. Lieber, Appl. Phys. Lett. **78**, 2214 (2001).
[31] H. Adhikari, A. F. Marshall, I. A. Goldthorpe, C. E. D. Chidsey, and P. C. McIntyre, ACS Nano **1**, 415 (2007).
[32] G. E. Jellison, Jr., Appl. Opt. **30**, 3354 (1991).
[33] S. Sade, L. Nagli, and A. Katzir, Appl. Phys. Lett. **87**, 101109 (2005).